

A Single-Channel Implantable Microstimulator for Functional Neuromuscular Stimulation

Babak Ziaie,* *Associate Member, IEEE*, Mark D. Nardin, Anthony R. Coghlan, *Member, IEEE*, and Khalil Najafi, *Member, IEEE*

Abstract—This paper describes a single-channel implantable microstimulator for functional neuromuscular stimulation. This device measures $2 \times 2 \times 10 \text{ mm}^3$ and can be inserted into paralyzed muscle groups by expulsion from a hypodermic needle. Power and data to the device are supplied from outside by RF telemetry using an amplitude-modulated 2-MHz RF carrier generated using a high-efficiency class-E transmitter. The transmitted signal carries a 5-b address which selects one of the 32 possible microstimulators. The selected device then delivers up to $2 \mu\text{C}$ of charge stored in a tantalum chip capacitor for up to $200 \mu\text{s}$ (10 mA) into loads of $< 800 \Omega$ through a high-current thin-film iridium-oxide (IrOx) electrode ($\sim 0.3 \text{ mm}^2$ in area). A bi-CMOS receiver circuitry is used to: generate two regulated voltage supplies (4.5 and 9 V), recover a 2-MHz clock from the carrier, demodulate the address code, and activate the output current delivery circuitry upon the reception of an external command. The overall power dissipation of the receiver circuitry is 45–55 mW. The implant is hermetically packaged using a custom-made glass capsule.

Index Terms—Biotelemetry, functional electrical stimulation, implantable devices, medical microsystems, rehabilitative devices.

I. INTRODUCTION

THE ABILITY to electrically stimulate selected groups of neurons in the central and peripheral nervous system has proven to be an effective way to intervene in a variety of neurological disorders [1]. Over the years, researchers and clinicians have used electrical stimulation to provide controllable limb function in paraplegics and quadriplegics [2], sensation of sound in the profoundly deaf [3], perception of light spots in the visually impaired [4], and suppression of intractable pain [5]. When electrical stimulation is used to stimulate motor neurons and elicit controllable muscle contractions, it is called functional neuromuscular stimulation (FNS). These electrical stimuli are applied to various muscle groups through appropriate electrodes which are connected to a stimulator circuitry. The circuitry can either be located outside

the body and connected to the electrodes via percutaneous electrical wires (nonimplantable) or be implanted inside the body along with interconnect cables (implantable). Implantable devices have been powered typically by either a small battery or an inductively coupled link, depending on the power requirement and lifetime of the device [6].

Over the last two decades, three generations of FNS systems have been developed and used with various degrees of success. In the first generation, the stimulator circuitry was constructed using discrete devices assembled on medium-sized boards using various hybrid techniques. This resulted in large systems that were not suitable for implantation and, consequently, were connected to the stimulating electrodes by percutaneous wires [7], [8]. In this technique the lead wires were prone to flexion fatigue and breakage, and could cause mechanical trauma and infection at the site of entry through the skin. In addition, percutaneous wires were not cosmetically acceptable for most patients. The second generation systems used microelectronics techniques to reduce the stimulator dimensions and to make the device more suitable for implantation [2], [9]–[13]. Several multichannel stimulators were developed that used a centrally located (abdominal cavity for lower extremity and shoulder region for upper extremity) package containing the circuitry and hybrid components. This central module was connected to distant sites by long cables and lead wires. However, designing and implanting the extensive wiring and cabling systems in multichannel applications is a challenging problem. The third and most recent group of devices are single-channel implantable stimulators [14]. These devices have used microelectronics techniques and miniature hybrid surface-mount components to create a small single-channel unit that can be implanted in numerous quantities near the individual targets. Since these devices use traditional glass sealing and metal-glass feedthrough techniques, it is difficult to expand them to a multichannel system.

This paper describes the development of an implantable, single-channel microstimulator that belongs to the third generation of FNS systems [15]. We have used miniature hybrid components along with microelectronics technology to develop a device small enough to be implanted through a gauge-12 hypodermic needle (outer diameter = 2.75 mm, lumen diameter = 2.15 mm). Fig. 1 shows the overall structure of the device. The microstimulator receives power and data through an inductively coupled link and has overall dimensions of $2 \times 2 \times 10 \text{ mm}^3$. It consists of: 1) a silicon substrate

Manuscript received May 17, 1996; revised May 5, 1997. This work was supported by the Neural Prosthesis Program, National Institutes of Health, under Contracts NIH-N01-NS-4-2319, NIH-N01-NS-1-2314, and NIH-N01-NS-8-2312. Asterisk indicates corresponding author.

*B. Ziaie is with the Center for Integrated Sensors and Circuits, Department of Electrical Engineering and Computer Science, University of Michigan, 1301 Beal Ave., Room 1246, Ann Arbor, MI 48109-2122 USA (e-mail: babak@engin.umich.edu).

M. D. Nardin, A. R. Coghlan, and K. Najafi are with the Center for Integrated Sensors and Circuits, Department of Electrical Engineering and Computer Science, University of Michigan, Ann Arbor, MI 48109-2122 USA.

Publisher Item Identifier S 0018-9294(97)06896-1.

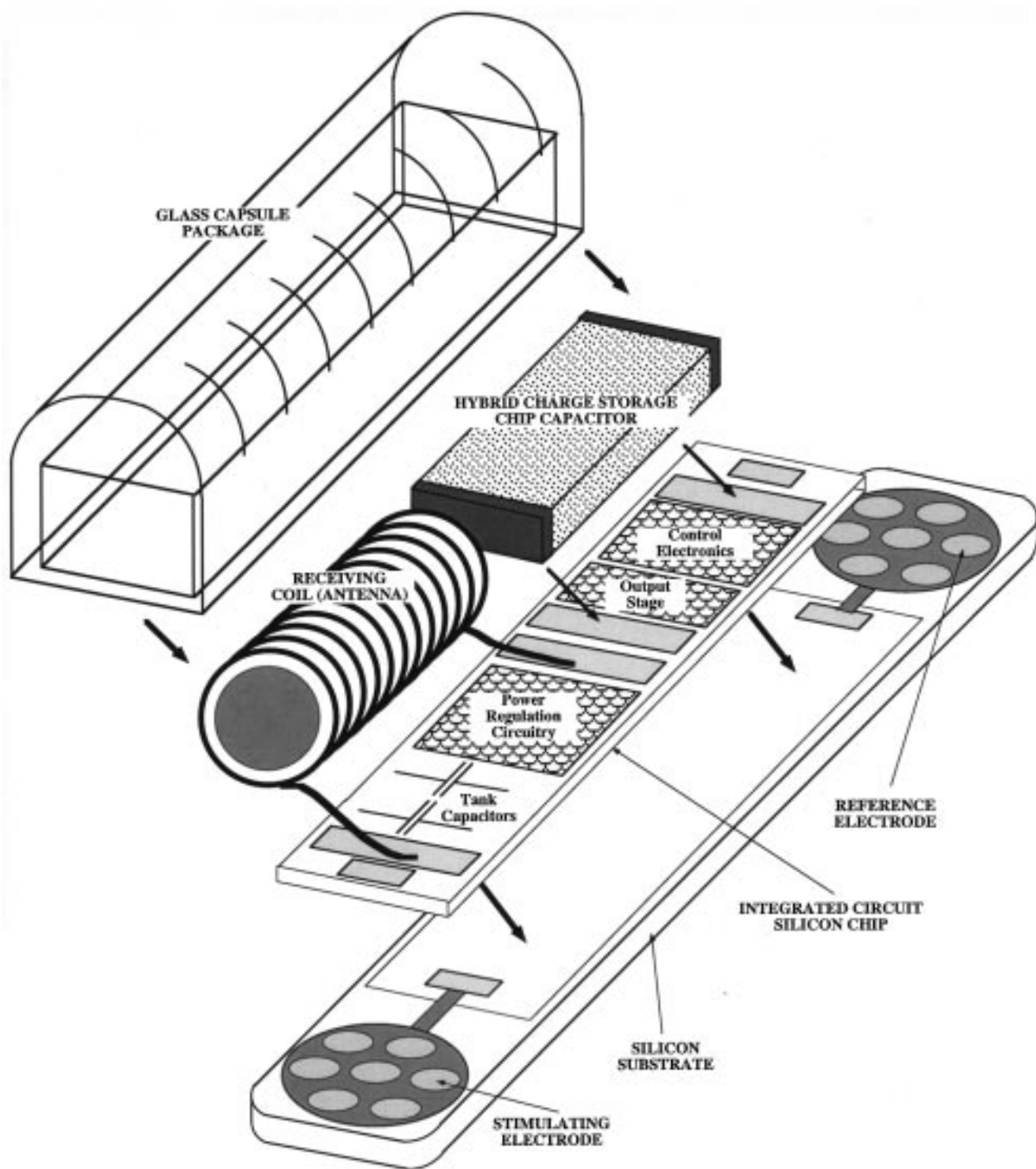


Fig. 1. Overall structure of a single-channel implantable microstimulator.

supporting a stimulating electrode at each end and providing multiple feedthroughs, 2) a receiver circuit chip, 3) a hybrid capacitor used for charge storage of the stimulation pulse, 4) a hybrid receiver coil for power and data reception, and 5) a custom-made glass capsule which is electrostatically bonded to the substrate to protect the receiver circuitry and hybrid elements from body fluids (the device should remain functional for 40 years). By using a hermetic silicon-glass packaging

technique with multiple feedthroughs, it is possible to increase the number of stimulation channels in future systems (this can be done by increasing the length of the silicon substrate and placing more electrodes on it).

In Section II the microstimulator system architecture is discussed, followed by a description of the transmitter circuitry and inductive link in Section III. Various building blocks of the receiver circuitry and its fabrication technology are described

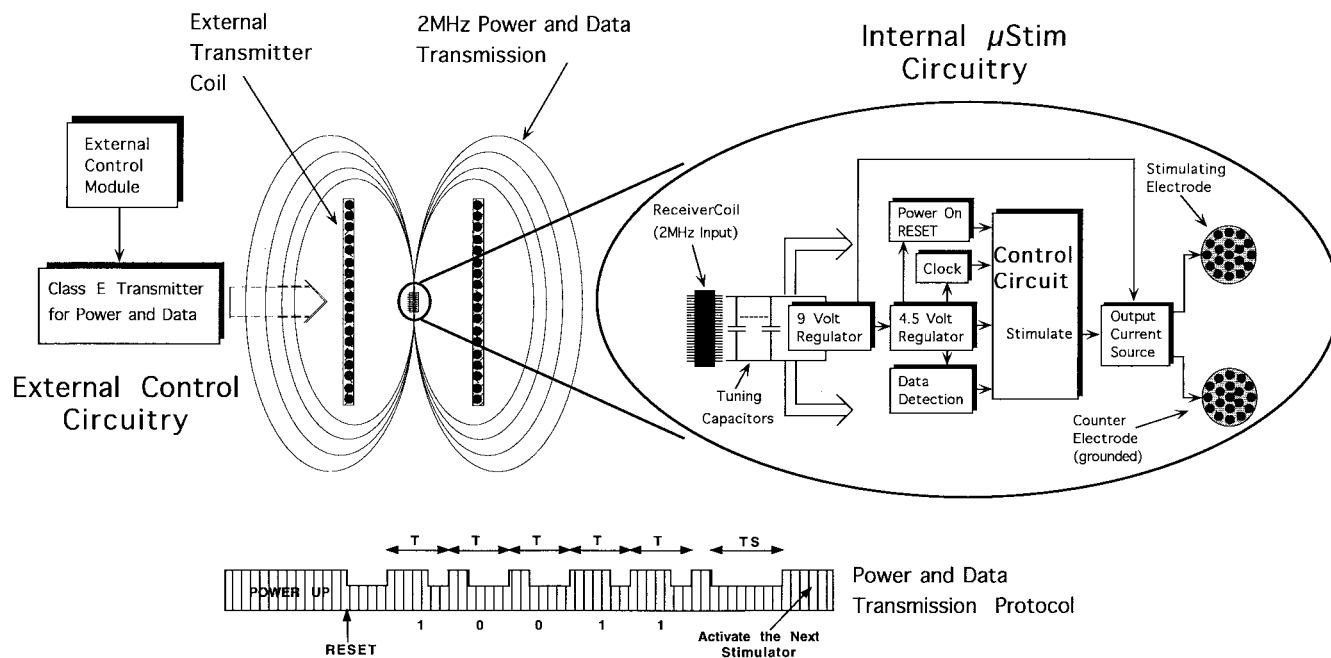


Fig. 2. System block diagram and data transmission protocol for a 5-b addressable single-channel microstimulator.

in Section IV. In Sections V and VI the electrode and package design are briefly discussed. Sections VII and VIII describe the assembly technique and test results, respectively. Finally, Section IX draws some conclusions from the results of this work.

II. SYSTEM ARCHITECTURE

Fig. 2 shows the overall system block diagram and data transmission protocol for a 5-b addressable single-channel microstimulator. As was mentioned previously, the device receives power and data through RF telemetry. This is achieved by amplitude modulation of a 2-MHz carrier. The choice of the carrier frequency is dictated by a tradeoff between adequate miniaturization of the components (mainly, receiver coil and tuning capacitors) and tissue absorption of the electromagnetic energy. A 2-MHz carrier allows adequate miniaturization while permitting enough power to be transmitted to the receiver without much RF absorption and tissue heating (see Section III). The telemetry link is a transformer-like coupled pair of coils that has been previously used in implantable telemetry applications [6]. In order to supply enough power to the receiver coil, a high-efficiency transmitter/amplifier was used. Class-E power amplifiers show efficiencies in the 80–100% range and are suitable for this application where the coupling between the transmitter and receiver is very weak [16], [17]. We will discuss the operation of the class-E power amplifier in Section III.

The receiver-stimulator circuit design depends primarily on the data/power transmission format chosen for the microstimulator. The flow of data and power from the time that the transmitter is turned on is illustrated in Fig. 2 and can be summarized as follows. After power-on, the carrier amplitude is momentarily turned low to reset all of the blocks on the receiver chip and is then amplitude modulated to transmit a

5-b address to as many as 32 microstimulators located within the volume of the transmitter coil (this coil is 9 cm in diameter and 8.5 cm long). After a specific microstimulator is selected, the carrier signal is turned high and then back low again. It is maintained at this low level for a period of up to 200 μ s. The selected microstimulator will then deliver a constant current pulse of 10 mA into loads of $<800 \Omega$ through the stimulating electrode pair for the period of time that the carrier is low [18]. Finally, the carrier is turned back high again, which will indicate the end of the stimulation period to the selected microstimulator.

The receiver circuitry for the microstimulator contains five main circuit blocks: two voltage regulators, an envelope detector for data demodulation, a clock recovery circuit, a control circuit, and an output pulse delivery circuit. The receiver coil picks up the amplitude-modulated RF carrier from the external transmitter and performs the following functions: 1) generates two regulated voltage supplies, one 4.5 V for the control circuitry and one 9 V for the output stage (delivering 10 mA of current into a load of $\leq 800 \Omega$ requires a supply voltage of at least 8 V); 2) charges a 1- μ F tantalum chip capacitor to the 9-V supply; 3) regenerates the carrier clock; 4) decodes the modulated carrier to recover the control data for use by the control circuitry; 5) compares the demodulated address code with the microstimulator internal identification code (which is programmed into the control circuitry by laser-trimming metal lines in the circuit); 6) sends a pulse (up to 200 μ s in duration) from the control circuit to the output circuit, signaling the stimulation period if the correct microstimulator has been selected; and 7) discharges the storage capacitor through the stimulating electrode and body tissue. At the end of the stimulation period, the storage capacitor is recharged to the 9-V supply. In Section IV we will describe various circuit blocks of the microstimulator receiver circuitry in more detail.

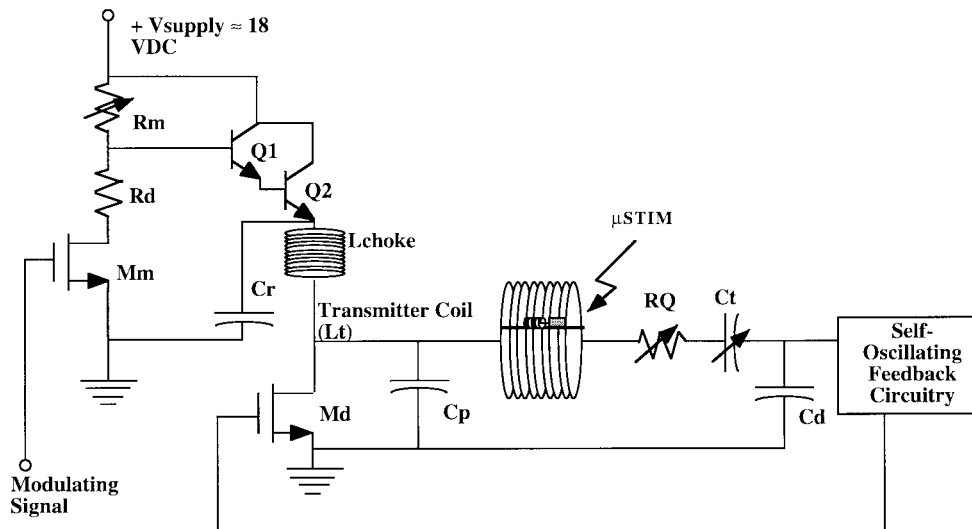


Fig. 3. The class-E amplifier is shown, with a microstimulator (with receiver coil mounted) inside the transmitter coil.

III. HIGH-EFFICIENCY CLASS-E TRANSMITTER

As was mentioned in Section II, the microstimulator is powered and controlled through an inductive telemetry link driven by a class-E power amplifier. The class-E amplifier is chosen because of its simplicity and very high efficiency [16]. This efficiency in the active device is necessary because the efficiency of the link is quite poor due to the very low coupling between the transmitter and receiver coils (with the implanted system receiving <1% of the average emitted RF energy). This low coupling results from the fact that the transmitter coil is essentially a relatively large air-core inductor, while the receiver coil is a much smaller coil with a cross section that does not capture a very large portion of the magnetic flux despite its ferrite core. It is beneficial, then, that in the class-E amplifier nearly all of the power drawn from the supply is radiated through the resonant loop with the external inductor coil forming the transmitting antenna.

Fig. 3 shows the class-E amplifier/transmitter with a microstimulator (with the receiver coil) inside the transmitter coil. The active device (M_d) is a high-speed power MOSFET that drives the resonant network consisting of parallel capacitor (C_p), transmitter coil (L_t), R_Q for limiting the Q of the transmitter's tuned network, and the capacitors C_t and C_d . Capacitor C_t is variable and is used for tuning the transmitter to the required carrier, while C_d forms a capacitive voltage divider with C_t in order to keep the input voltage to the self-oscillating feedback circuitry at safe levels (the purpose of this feedback circuitry will be discussed in greater detail). Typically, the resulting sinusoidal voltage and current in the transmitter coil are about 750-V and 0.5-A peak, respectively.

In the class-E power amplifier, the voltage across the inductor in the series load is a linear function of the supply voltage. In the microstimulator transmitter this principle is used to amplitude modulate the outgoing signal. The desired digital signal from a signal generator or external computer driver causes the amplifier to operate at one of two supply levels by turning on or off the linear switching MOSFET

(M_m), selectively incorporating or disabling a voltage divider formed by resistors R_m and R_d . By adjusting R_m , the degree of modulation is easily varied to accommodate the levels needed by the receiver's data detection circuitry. The Darlington pair formed by transistors Q_1 and Q_2 serves to buffer and translate the voltage shifts from the resistive divider into effective shifts in supply voltage for the class-E amplifier, while supplying ample current drive. The current is kept relatively constant by the use of a choke-inductor coil (Lchoke). Capacitor C_r helps to filter switching transients and ringing in the amplifier's supply voltage as the signal is modulated. Using a square wave as the incoming data signal, the transmitter has been found to respond to modulation frequencies up to 80 KHz, much faster than the data which is sent to the microstimulator in practice.

Mismatch between the switching frequency of the driving device and the resonant frequency of the load network will cause excessive power loss in the active device and may destroy the active device if this inefficient condition is prolonged. It is important to account for this mismatch, since it can arise quite naturally from the change in inductance of the transmitter coil due to coil warping from limb flexion, as well as from loading of the transmitter coil due to the proximity of other strong electromagnetic fields or ferromagnetic objects. The amplifier uses a custom CMOS-feedback system to automatically adjust the driving device's frequency to that of the resonant network. In this manner, damage to the driving device and failure of the system are prevented. The feedback is also responsible essentially for starting the amplifier upon power-up, since the first oscillations in the resonant network are fed back to the driving MOS (M_d) with the appropriate phase to cause it to start switching at the tuned network's frequency, until the oscillations quickly become self-sustained. The feedback has been shown to work within a wide range of coil warping. Looking at the transmitter coil along its axis, so that its cross section is increasingly elliptical as it is distorted, and defining the coil aspect ratio as the ratio of the length of the

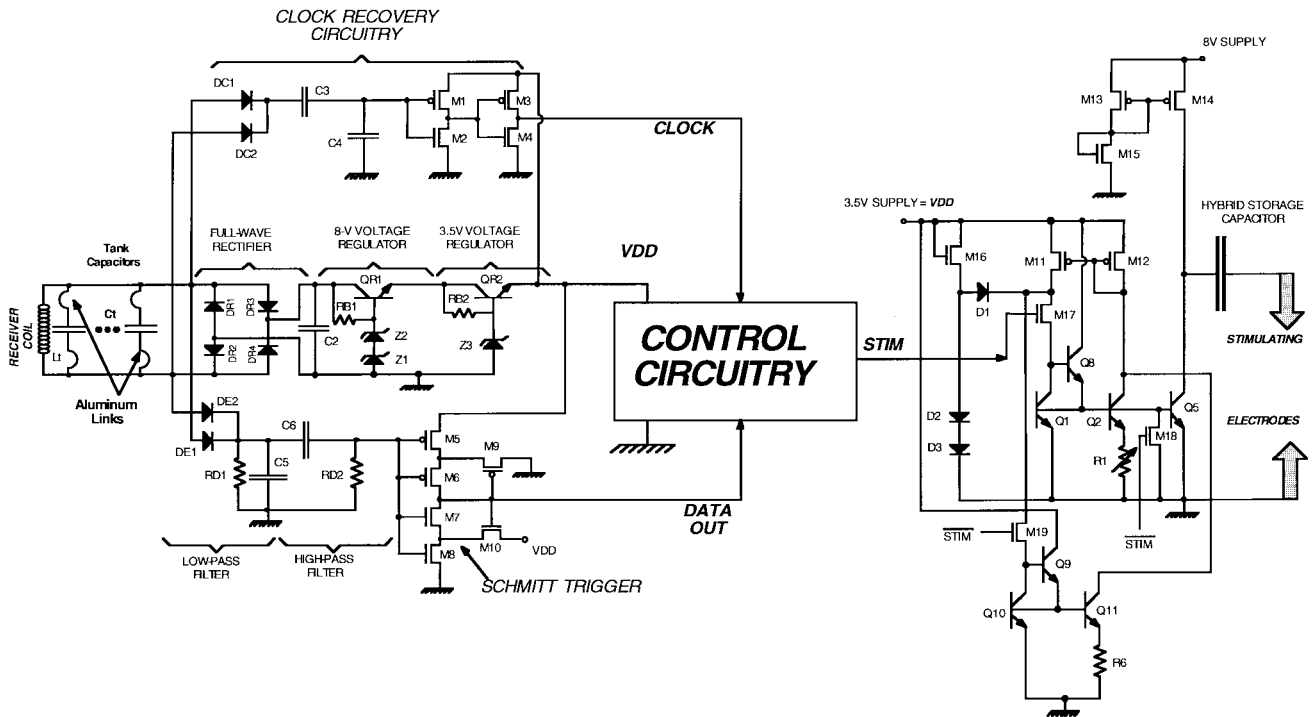


Fig. 4. Single-channel microstimulator system electronics.

major axis to the length of the minor axis, it has been observed that this ratio can reach approximately four (i.e., the coil can be significantly flattened and distorted) before potentially damaging deviation occurs from the normal class-E behavior. At this point, the transmitted voltage actually remains about 80% of its peak value, and the frequency has increased about 17% from its ideally tuned value (2 MHz, in this case). It is unlikely that such severe distortion will occur in normal use, and the receiver's Q is typically low enough that the shift in frequency will not significantly affect power reception.

A strong magnetic field associated with the transmitter coil can induce electric field (E) and current (J) in the tissue. Thermal effects of RF fields in tissue (with conductivity σ) arise due to the ohmic loss ($1/2 \sigma E^2$) associated with the induced electric field. This can cause excessive heating and damage if not kept below a certain limit. The safe limit is usually considered to be the basal metabolic rate (~ 1 W/Kg) above which any heating would be undesirable [19]. For a single-layer transmitter coil with 46 turns (N), 9 cm in diameter ($2a$), and 8.5 cm in length (d) used in our experiments (see Section VIII) the axial magnetic field ($B_z = \mu_0(NI/2a\sqrt{1+(d/2a)^2})$) can be calculated to be 2.3×10^{-4} T (current = 0.5 A) [20]. Using quasistatic approximation, this magnetic field induces a transverse electric field ($|E_\phi| = \omega Br/2$, where r is the radial distance from the axis of the coil and ω is the angular frequency) of ~ 44 V/m at a distance of 3 cm from the coil's axis at 2 MHz. As can be seen, the induced electric field is zero at the center of the transmitter coil and increases toward the perimeter. A distance of 3 cm from the center of a 4.5-cm radius coil is a good location to calculate maximum field in the muscle tissue since the remaining distance is skin, fat, and connective tissue

having lower conductivity. The muscle tissue conductivity in transverse direction (this is the same direction as the induced electric field) at 2 MHz is 0.5 S/m [21], which amounts to a power dissipation of ~ 0.5 W/Kg (muscle tissue density is ~ 1 g/cm³ [22]). This is below the safe exposure limits and would not cause any problem. The conductivity of skin and fat tissue is even lower than muscle and, therefore, the power dissipation in those tissues is even smaller than 0.5 W/Kg.

IV. RECEIVER CIRCUITRY AND FABRICATION TECHNOLOGY

Fig. 4 shows the overall diagram of the microstimulator receiver circuitry, which consists of five major subcircuits, as discussed below.

A. Voltage Regulator Circuitry

The received signal after being picked up by a resonant tank circuit (L_t, C_t), goes through a full-wave rectifier and two series voltage regulators in order to generate the required supply voltages. The tank circuit consists of an inductor ($L_t = 40$ – 80 μ H and $Q_t = 30$ – 60 at 2 MHz), which is wound over a ferrite core (Section VII) and a series of parallel connected on-chip capacitors with appropriate trimmable aluminum links (individual circuits can be trimmed for the desired received frequency). The voltage regulators consist of a full-wave bridge rectifier (DR₁–DR₄, BV = 50 V), storage capacitor (C₂, 270 pF), and 4.5-V and 9-V shunt regulators (QR₁ and QR₂, $\beta_F = 200$) implemented using Zener diodes (Z₁ – Z₃, $V_Z = 5.2$ V and $I_Z = 600$ – 800 μ A) and resistors (RB₁ and RB₂ = 7.5 K Ω). The two main design considerations for the voltage regulation circuitry are preventing device breakdown due to the high input voltages received by the

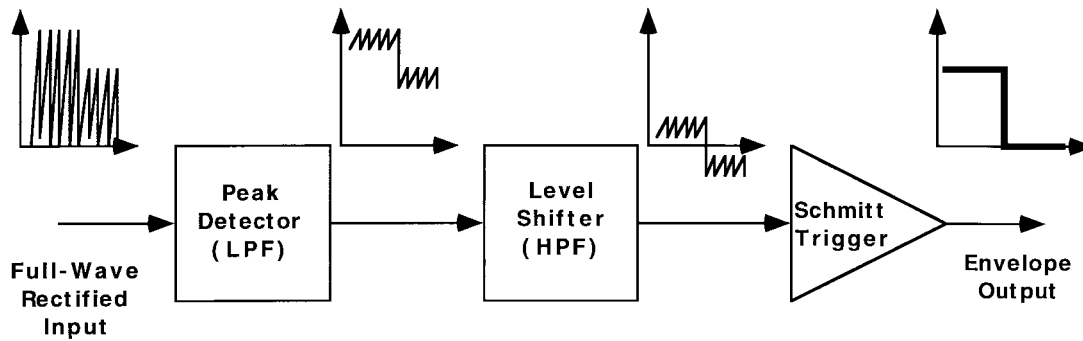


Fig. 5. Block diagram illustrating the operation and waveforms in the AM envelope detector.

solenoid coil (as high as 20–30 V), and providing good dc regulation from the 2-MHz carrier. Bipolar transistors and diodes with high breakdown voltages are used to provide protection from high input voltages. DC regulation is achieved by passing current through Zener diodes to provide a reference voltage, and by using n-p-n bipolar transistors as current drive devices. Due to the sharp relationship between current and voltage in Zener diodes, they provide a stable and reproducible reference voltage, and the high current gain of the n-p-n bipolar transistors provides a voltage source with a very low output resistance that can supply a stable output voltage to a variable load.

B. Clock Recovery Circuitry

The clock is regenerated from the RF carrier by taking the 12–20-V peak amplitude, 2-MHz sinusoidal carrier input and generating a 4.5-V square wave output. The design considerations for this circuit are to provide breakdown protection from the high input voltages and to obtain a clock with 50%-duty cycle from the sinusoidal input. Voltage protection is provided by using p-n junction diodes (DC_1 and DC_2 , $BV = 50$ V) followed by a capacitive voltage divider (C_3 and C_4) to provide full-wave rectification and to attenuate the peak input voltage to <9 V. Two cascaded CMOS inverters (M_1 – M_4) are then used to buffer this ac signal and produce the clock signal used by the rest of the circuitry.

C. Data Detection Circuitry

Fig. 5 shows the block diagram for a general AM envelope detector and various waveforms as the received amplitude-modulated carrier passes through the data-detection circuitry. The data recovery circuit is comprised of three main parts: a lowpass filter (LPF), a highpass filter (HPF), and a Schmitt trigger for envelope detection and noise suppression. The lowpass filter is necessary in order to extract the envelope from the 2-MHz carrier, as illustrated in Fig. 5. This filter is constructed using diodes DE_1 and DE_2 , resistor RD_1 (50 K Ω), and capacitor C_5 (90 pF). The diodes are used to detect the peaks of the envelope, with RD_1 and C_5 determining the corner frequency of the LPF. The highpass filter is a standard RC circuit consisting of capacitor C_6 (90 pF) and resistor RD_2 (500 K Ω) and is required to remove the dc offset of the envelope and provide breakdown protection for the CMOS

gate inputs of the Schmitt trigger. The Schmitt trigger has to produce a 0–4.5-V output signal that accurately follows the envelope at its input in the presence of noise. The Schmitt trigger is comprised of transistors M_5 – M_{10} , with M_9 and M_{10} providing current feedback. The dimensions of M_9 and M_{10} are set to determine the threshold levels of the hysteresis provided by the Schmitt trigger (0.5 V and 1.7 V).

D. Output Current Delivery Circuitry

The requirements for the output current delivery circuitry are to provide a cathodic first constant current pulse with fast rise and fall times for the entire pulse duration, and to charge-balance the storage chip capacitor during the time between two consecutive stimulating pulses. The output circuit contains charge-balance circuitry, stimulus current regulator circuitry, and startup circuitry.

The charge-balance circuitry provides a current of 100 μ A through the M_{13} – M_{14} – M_{15} current mirror with M_{15} providing a reference current of 50 μ A and M_{14} being twice the size of M_{13} . The stimulus current regulator circuitry generates a stable and supply independent current pulse. This was accomplished by using a thermal voltage reference current source ($V_T = 26$ mV at room temperature) [23]. Transistors Q_1 and Q_2 , and resistor R_1 are used to create this stable stimulus pulse. With the area of Q_1 being half the area of Q_2 , the voltage drop across R_1 is $V_{R1} = V_T \ln(2)$, this produces a reference current of $I_{Q2} = (V_T/R_1) \ln(2)$ in Q_2 . As can be seen, this reference current is independent of power-supply voltage and is only proportional to V_T , R_1 , and the ratio between the emitter areas of Q_1 and Q_2 . In the microstimulator design the collector current in transistors Q_1 and Q_2 is set at 50 μ A by choosing appropriate value for R_1 (360 Ω). Transistor M_{17} is used to switch this reference current on and off, while M_{11} – M_{12} are used to provide a constant load. The drive transistor is Q_5 and has an area of 200 times that of Q_1 in order to provide the constant current drive of 10 mA through the electrodes. Transistor M_{18} is used to achieve faster switching times and aid in charge removal from the base of the drive transistor. Transistors M_{19} , Q_9 – Q_{11} , and resistor R_6 are used to maintain a constant load current for the M_{11} – M_{12} current mirror when no pulse is delivered to external electrodes. The startup circuitry consists of transistor M_{16} and diodes D_1 – D_3 , which will prevent the circuit from

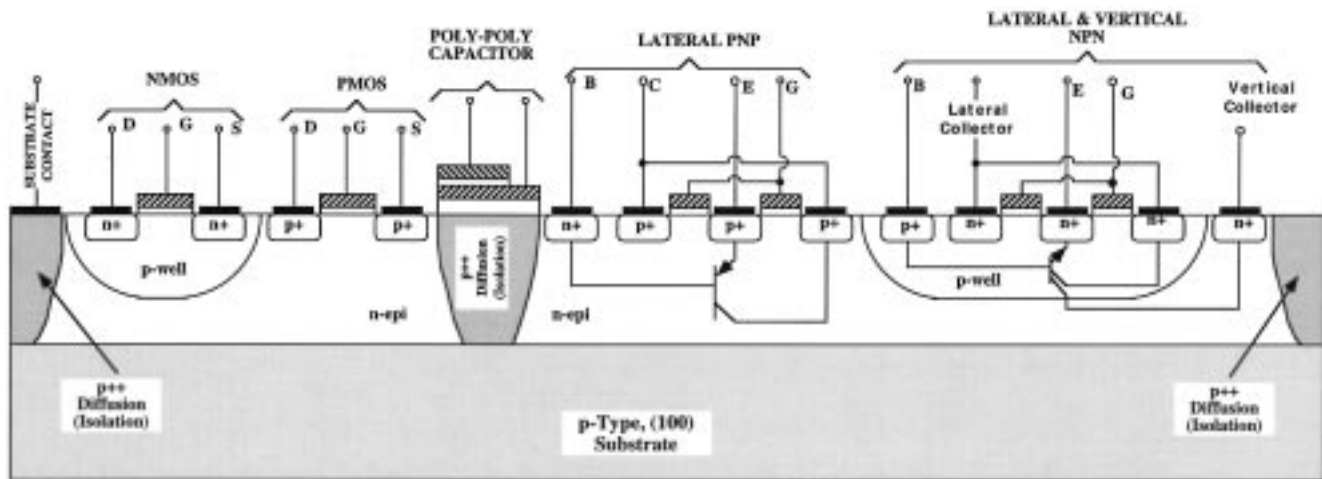


Fig. 6. Cross-sectional view of the bipolar-CMOS fabrication technology.

remaining in a stable state in which zero current flows in the circuit, even when the power supply voltage is nonzero [23].

The maximum stimulation frequency (or minimum inter-pulse delay) is a function of the amount of injected charge per stimulation period, the magnitude of the charge-balance current, and the time required to send the address data stream. This is to ensure that the electrodes are charge balanced at the end of each stimulation period. In our design, the charge current is fixed at $100 \mu\text{A}$, therefore, with a minimum stimulation duration of $10 \mu\text{s}$ (see Table I) at 10-mA stimulation current level and a $100\text{-}\mu\text{s}$ period for each address bit, one cannot increase the stimulation frequency beyond 600 Hz. The charge-balance circuitry can be easily redesigned to generate a variable charge-balance current level and accommodate a higher stimulation frequency (600 Hz would be more than adequate for most applications).

E. Control Circuitry

The control circuitry receives the unsynchronized envelope detector output and clock from the input circuitry. It generates a synchronized output and detects the logic ones and zeroes used to represent the address of the microstimulator. A zero is differentiated from a one by the duration of a high pulse. The minimum clock count necessary to register a one is programmable. Each microstimulator also has five address bits which are programmable. Following synchronization, the received address bits are sequentially shifted into a 5-b register which is controlled by a 3-b state counter. The contents of this address shift register are compared with the programmed address of the stimulator to enable the stimulus control. The duration of the next low pulse received from the transmitter will determine the duration of the stimulus pulse. Upon completion of the stimulus pulse, the circuitry resets all of the counters and awaits the receipt of another address.

F. Fabrication Technology

As can be seen from the above discussion, a variety of passive and active devices are used in the implementation of the receiver circuitry, including MOS and bipolar transistors, p-n junction diodes, Zener diodes, resistors, and capacitors. In

TABLE I
SUMMARY OF MEASURED PERFORMANCE CHARACTERISTICS OF
THE SINGLE-CHANNEL MICROSTIMULATOR RECEIVER CIRCUITRY

Parameter	Value
Operating Frequency	2 MHz
Received Voltage	10–21 V
Regulated Received Voltages	9 ± 0.5 and 4.5 ± 0.2 V
Modulation Depth	3 V
Stimulation Duration	10–200 μs
Stimulation Frequency	≤ 40 Hz
Stimulation Current Amplitude	10 mA
Load Resistance	$\leq 800 \Omega$
Power Consumption (at 20 V Received Voltage)	45–55 mW
Area	$1.36 \times 7.5 \text{ mm}^2$
Technology	3 μm , bi-CMOS

previous implantable stimulators, many of these elements were hybrid components which took up large amounts of space. For the microstimulator, the hybrid chip capacitor and receiving coil consume most of the available volume, so the rest of the stimulator circuitry must be made very small and without hybrid components. We have developed a versatile fabrication technology that can be used to implement the required circuits [24], [25]. Fig. 6 shows a cross-sectional view of the device structures that can be implemented using this technology. The fabrication process combines deep-boron diffusion and a standard $3\text{-}\mu\text{m}$ p-well CMOS technology to implement a variety of active devices and passive components. The deep-boron diffusion penetrates through the n-epi layer and connects to the underlying p substrate, thus, creating junction isolated n-epi regions. In addition to CMOS circuitry (NMOS and PMOS transistors with threshold voltages of $+0.9$ and -0.9 V, respectively), the lightly-doped n-epi regions can house a number of different bipolar device structures. The process provides vertical n-p-n transistors ($\beta_F = 200$) in the isolated n-epi regions and a number of junction diodes (p-well/n-epi diodes, p-well/n⁺ diodes, or p⁺/n⁺ Zener diodes). In addition to active devices, the fabrication process provides two layers of polysilicon for fabrication of on-chip capacitors and a variety of diffused regions for forming large resistors. The fabrication

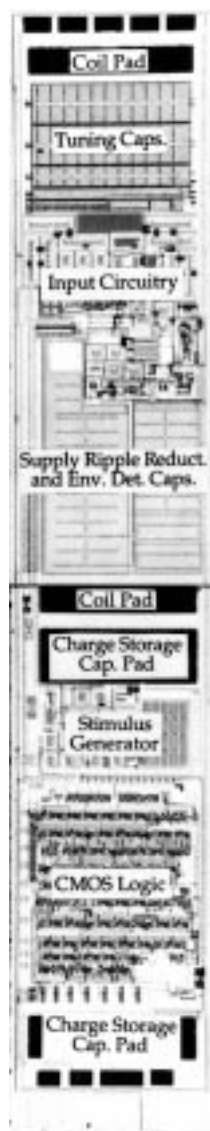


Fig. 7. Photograph of fabricated receiver circuitry, which measures 1.36×7.5 mm.

process requires a total of nine masking steps. Fig. 7 shows a photograph of the fabricated receiver circuitry ($1.36 \text{ mm} \times 7.5 \text{ mm}$).

V. STIMULATING ELECTRODES

As was mentioned in Section II, the microstimulator electrode should be capable of injecting $2 \mu\text{C}$ of charge in $200 \mu\text{s}$ (10 mA) through a small area designated to it (0.3 mm^2). This is a large amount of charge and conventional electrode materials (e.g., platinum and stainless steel) are unable to inject this amount of charge through such a small area without causing irreversible electrochemical reactions and gas evolution. This is due to their low charge injection capability (e.g., $25\text{--}75 \mu\text{C}/\text{cm}^2$ for platinum electrodes). In addition, simple planar electrodes show a drastic increase in current density around their perimeter (edge effect) [26]. This can drive the high current density regions beyond the safe electrochemical limits and delaminate the electrode material.

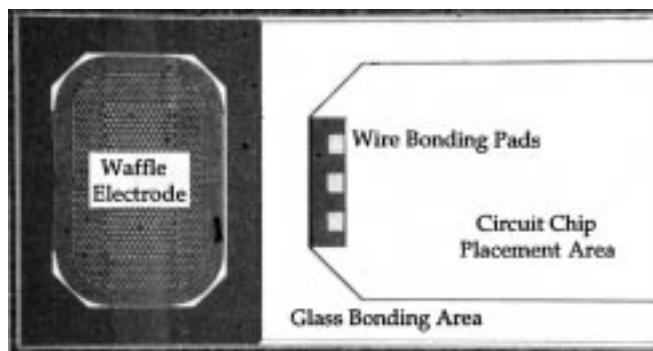


Fig. 8. Photograph of a high-current thin-film stimulating microelectrode.

Anodically prepared IrOx film has attracted much attention as a high charge injection capability material suitable for small stimulating electrodes [27]. This is due to its high charge injection capacity (at least $3\text{--}5 \text{ mC}/\text{cm}^2$ geometric area), nontoxicity, and compatibility with integrated circuit (IC) fabrication technologies. IrOx injects charge through faradaic processes of valence transitions and proton or hydroxyl ion transfers that occur within the multilayer IrOx film. These chemical reactions coupled with the porosity of the IrOx film are responsible for its high charge injection capacity. IrOx was chosen for the microstimulator electrode material due to its large charge injection capability.

In order to overcome the edge effect, a new waffle-shaped thin-film electrode has been designed that reduces the current density around the perimeter by dividing the total area into many small sites ($10 \mu\text{m}$ in diameter) connected in parallel, each one carrying a portion of the total current (Fig. 8). This has a twofold effect on electrode performance. First, multiple small sites each have higher impedance than a single large site and as has been shown this creates a more uniform current distribution on each site [28]. Second, the larger the recess to radius ratio in a recessed electrode, the more uniform is the current distribution [29]. The thin-film waffle electrodes are recessed in a dielectric which is $0.8\text{-}\mu\text{m}$ thick. This means that the smaller sites have a larger recess to radius ratio than a larger electrode and this further improves the current density distribution. These electrodes have been tested with 10-mA current pulses in phosphate-buffered saline (PBS) and are able to withstand more than two billion current pulses without any sign of degradation (a total of 16.8 billion pulses are required for 8-h/day operation and 40-years lifetime at 40-Hz stimulation rate) [30]. These waffle electrodes are integrated on the silicon substrate which supports the receiver circuit chip, and are located at the two ends of the substrate (Fig. 1).

VI. HERMETIC PACKAGING

Hermetic packaging of implantable devices is a challenging problem. The microstimulator receiver circuitry and hybrid components must be protected from body fluids for 40 years. We have developed a new packaging technique that uses a high-yield, low-temperature ($320 \text{ }^\circ\text{C}$) electrostatic (anodic) bonding of a custom-made glass capsule (Corning #7740, $2 \times 2 \times 8 \text{ mm}^3$) to fine-grain polysilicon in order to form

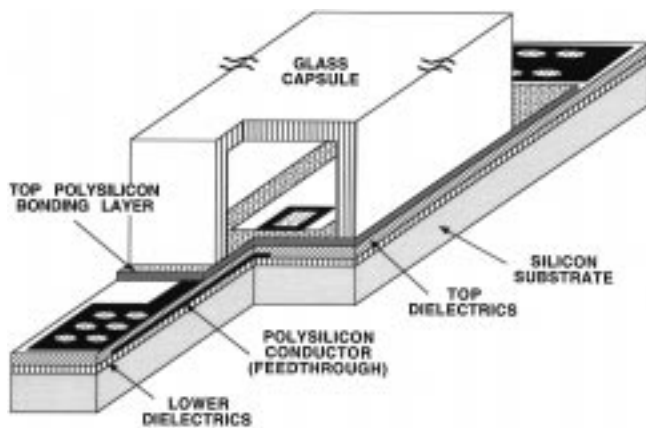


Fig. 9. The microstimulator packaging structure.

a hermetically sealed cavity (Fig. 9). Anodic bonding is a very simple technique that requires heating the glass capsule and the silicon substrate to ~ 320 °C while keeping glass at a negative potential of ~ 2000 V with respect to the silicon substrate [31]. This generates a high electric field at the glass-silicon interface and causes a chemical bond between silicon and glass. The bonding temperature was kept low by using a polysilicon overlayer, thus, reducing the damage that can be caused to the hybrid elements [32].

The stimulating electrodes outside the package were connected to the receiver circuitry inside by using a new feedthrough technique [33]. This technique uses closely spaced polysilicon lines that are covered by phosphosilicate glass (PSG). The planarity over the feedthrough lines is critical for a successful bond, since any step over the lines prevents a good bond and can cause moisture leakage inside the package. In order to produce a planar surface on top of the feedthrough lines, the PSG is annealed in steam at 1100 °C (this causes the PSG to soften and flow) [34]. The multiple-feedthrough technique is an attractive feature of the microstimulator, since it will allow expanding the single-channel device to a multichannel one without any added process complexity. We have also incorporated a dew-point sensor inside the package to monitor any moisture condensation during soak tests. Saline and deionized (DI) water soak tests at elevated temperatures (85 °C and 95 °C) were performed to determine the reliability of the package. Preliminary results have shown a mean time to failure (MTTF) of 284 days and 118 days at 85 and 95 °C, respectively, in DI water. An arrhenius-diffusion model for moisture penetration yields an expected lifetime of 116 years at body temperature (37 °C) for these packages [33].

VII. ASSEMBLY

In order to maximize the yield of complete, fully functional microstimulators, it was necessary to develop an assembly procedure that could be implemented reliably and without considerable difficulty. The microstimulator receiver circuitry and substrate containing the stimulating electrodes are fabricated separately. The fabricated receiver chips are diced from the wafer and separated from each other. They are then extensively tested and cleaned along with electrode substrates

before assembly. In order to avoid contaminating the bond area on the substrate during assembly, the inductor and chip capacitor are first mounted on the circuit chip. The inductor is made of copper wire (AWG 43) which is wound on a ferrite core (1 mm in Diameter, 3-mm length, $\mu = 125$) and set in place with polyimide (PI2611 DuPont, Wilmington, DE). It measures about 1.25 mm (diameter) \times 3 mm (length) and has an inductance and Q of about 40–80 μ H and 30–60 (at 2 MHz), respectively. After the coil's insulation is stripped at the end of the windings, it is positioned carefully alongside the circuit under a microwelder. Each lead is then microwelded to its respective copper-electroplated pad on the circuit chip. The charge storage capacitor (0.7–1.0 μ F) is now attached to the circuit chip using conductive modified polyimide. Following the inductor and chip capacitor attachment to the circuit chip a fine line of polyimide is applied to the region of the electrode substrate on which the receiver chip will rest and the circuitry is carefully positioned on this region so that no polyimide or other contaminants pollute the anodic bonding region of the electrode substrate. After the circuit placement on the substrate, the polyimide is cured at 180 °C for 1 h. Finally, the circuit is electrically connected to the substrate by wire bonding, one bond for each electrode and one for the circuit's logic output for verification of functionality in further testing.

The almost complete unit is now ready for anodic bonding of the protective glass capsule over the circuit to the electrode substrate. First the assembled substrate, circuit chip, and glass capsule are cleaned using an acetone, isopropyl alcohol, and deionized-water rinse sequence. They are then placed in an oven at 200 °C for 24 h in order to allow the polyimide and various components to outgas adequately, as well as to evaporate moisture from the assembly. The glass capsule is then bonded to the substrate assembly on a hot plate at 320 °C by applying 2000 V for about 10 min. The assembled unit is attached with epoxy to a small printed circuit board that provides a means of testing the microstimulator for proper telemetric functionality after assembly and also for activating the high current density IrOx electrodes. The appropriate connections from the electrode substrate to the test board are wire bonded. It should be noted that it can be verified with considerable certainty that the circuit is still fully functional by monitoring the logic circuitry's output in response to the appropriate telemetrically sent signals once the test board-mounted device is telemetrically powered. Once the electrodes are activated, the microstimulator is separated from the test board by scribing the electrode substrate between the electrode closest to the end pads used for wire bonding to the board. Fig. 10 shows a photograph of a completely assembled single-channel microstimulator.

VIII. TEST RESULTS

The fabricated receiver circuitry was subjected to extensive bench tests to verify the individual building blocks and overall circuit functionality. A class-E power amplifier was used to transmit modulated data (see Section III) and drive the transmitter solenoid coil (single-layer, 46-turns, 9-cm diameter, 8.5-cm length, $L_t = 138$ μ H, $Q_t > 800$) at 2 MHz.

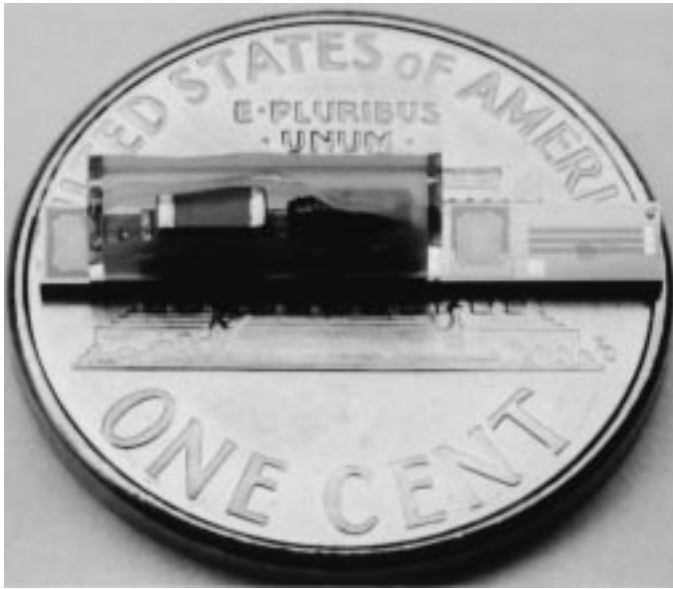


Fig. 10. Photograph of a completely assembled single-channel microstimulator.

The receiver circuitry mounted on the printed circuit board (Section VII) was then positioned inside the transmitter coil using a manipulator. Fig. 11 shows the voltage received by the microstimulator, demodulated data, and output stimulation pulse across a $680\text{-}\Omega$ load (output current $\sim 10.3\text{ mA}$). Table I summarizes the overall results from operation of a single-channel microstimulator. The experimental results for the 9-V and 4.5-V regulators showed a voltage ripple of $\pm 0.5\text{ V}$ and $\pm 0.2\text{ V}$, respectively. The operating range for the received input voltage is 10–21-V peak with 3-V modulation depth. The output of the data recovery circuit demonstrated a response time of $0.5\text{ }\mu\text{s}$ for the rising edge of the envelope and $9\text{ }\mu\text{s}$ for the falling edge. It was observed that the Schmitt trigger circuit had a hysteresis voltage of 1 V, had removed all high frequency ripple due to the RF carrier, and had generated a clean stable signal (Fig. 11). The overall power dissipation of the receiver circuitry was measured to be 45–55 mW (current consumption $\leq 3\text{ mA}$ at 20-V peak sinusoidal input voltage). About half of the power is consumed by the voltage regulators due to the design considerations to achieve the required regulation.

Power reception is dependent on both position and orientation of the implant within the transmitter coil. The receiver remained functional and was able to deliver the stimulating pulse in a volume of 320 cm^3 within the transmitter coil (volume bounded by a transverse plane about 1.25 cm from either ends). The received voltage dropped suddenly outside this volume. Misalignment of the receiver coil within the transmitter coil causes some power reception drop-off with a dependence somewhat looser than that expected strictly from the cosine of the angle of misalignment. Thus, the voltage received at a certain angle of axial misalignment (α) will exceed $V_{\text{max,PerfectAlignment}} \cdot \cos(\alpha)$. The electric field outside the coil diminishes inversely with respect to distance r ($|E_\phi| = \omega B a^2 / 2r$ [20]) and is equal to 3 V/m at a distance of 1 m. This is a large field and unless the transmitter coil

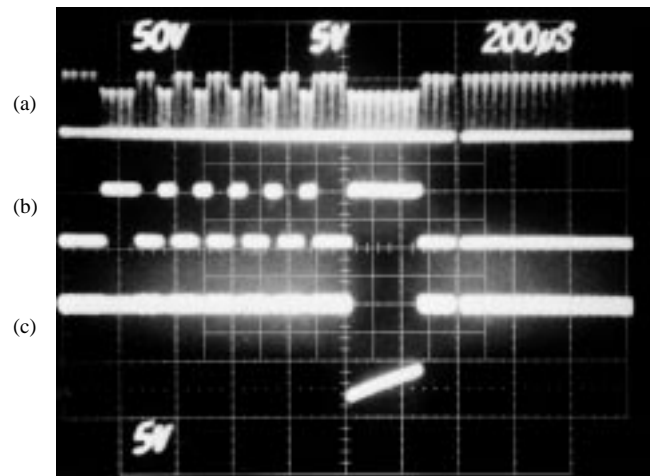


Fig. 11. Voltage received by the microstimulator [(a) input AM signal], (b) demodulated data, and (c) output stimulation pulse across a $680\text{-}\Omega$ load.

is properly shielded, it can cause interference in surrounding devices and instruments.

We have not performed *in vivo* tests on these microstimulators. Our *in vitro* test results regarding the four major parts of the microstimulator (i.e., class-E transmitter, receiver circuitry, high-current electrodes, and hermetic packaging) have shown that all these components are fully functional. However, *in vivo* functionality of the whole system has to be determined with animal tests. These tests require more sophisticated preparation and will have to be carried out in the future.

IX. CONCLUSION

We have developed a single-channel microstimulator for FNS applications. This device overcomes the shortcomings of previous neuromuscular stimulators by reducing the number of hybrid components, lead wires, and bulky packaging. The microstimulator is $2 \times 2 \times 10\text{ mm}^3$ in dimensions, requires only two hybrid components (a tantalum chip storage capacitor and a receiver coil), and can be injected into tissue by expulsion through a hypodermic needle, thus, reducing the risk and discomfort associated with surgical placement. The device receives power and data from outside by RF telemetry. A high-efficiency class-E amplifier/transmitter is used to transmit an amplitude-modulated 2-MHz carrier signal to the receiver. A custom-designed bi-CMOS receiver chip generates 9-V and 4.5-V-regulated supply voltages, demodulates control data from an amplitude-modulated RF carrier, regenerates a clock signal from the RF carrier, and delivers a constant current of 10 mA for durations up to $200\text{ }\mu\text{s}$ once commanded by the external transmitter. The circuitry has been fabricated using a $3\text{-}\mu\text{m}$ bi-CMOS fabrication technology and has been shown to be fully functional. The overall power dissipation of the receiver circuitry was measured to be 45–55 mW. A high-current iridium oxide thin-film microelectrode has also been developed as part of the microstimulator to enable the device to inject large amounts of charge ($2\text{ }\mu\text{C}$) through a small area ($\sim 0.3\text{ mm}^2$). These electrodes have been tested *in vitro* and have shown no sign of degradation after being subjected to more than two billion 10-mA current pulses. The device

is hermetically packaged in a custom-made glass capsule which is electrostatically bonded to a silicon substrate. The substrate contains stimulating electrodes and multiple high-density feedthroughs (200/mm) for connecting the receiver circuitry to the electrodes. Accelerated long term soak tests on these packages have shown an expected lifetime of 116 years at body temperature.

The overall system and individual circuit blocks developed for the implantable microstimulator will be applicable to a large class of devices which are remotely powered and controlled through RF telemetry (radio transponders and actuators). In some applications where the power demand is not as rigorous as in FNS, e.g., retinal and peripheral nerve stimulation, the hybrid coil and capacitor can be substituted by electroplated on-chip coil and thin-film capacitor. This will further reduce the size of the device and makes it more suitable for implantation in restricted anatomical regions. The microstimulator can also be expanded to a multichannel system by placing more electrodes on a longer substrate or using a flexible silicon ribbon cable with multiple electrodes. Cuff electrodes for peripheral nerve stimulation can also be fabricated along with the microstimulator. These future applications clearly demonstrate the possibility of using the versatile technologies developed for the microstimulator in other areas.

ACKNOWLEDGMENT

The authors would like to thank F. T. Hambrecht and W. Heetderks of the Neural Prosthesis Program, NINDS, for their encouragement and support throughout this work. They would also like to thank J. Von Arx and M. Dokmeci for their assistance in testing and fabricating electrodes and packages, Y. Gianchandani for designing the control circuitry, M. Putty and General Motors Research, Warren, MI, for their assistance in low-temperature oxide (LTO) and phosphosilicate glass (PSG) deposition, B. Casey for his help in assembly and packaging, and T. Hull for her assistance in fabrication.

REFERENCES

- [1] F. T. Hambrecht and J. B. Reswick, Eds., *Functional Electrical Stimulation, Application in Neural Prosthesis*. New York: Marcel Dekker, 1977.
- [2] J. R. Buckett, P. H. Peckham, G. B. Thrope, S. D. Braswell, and M. W. Keith, "A flexible, portable system for neuromuscular stimulation in the paralyzed upper extremity," *IEEE Trans. Biomed. Eng.*, vol. 35, no. 11, pp. 897-904, Nov. 1988.
- [3] F. B. Simons, "Electrical stimulation of the auditory nerve in man," *Arch. Otolaryng.*, vol. 84, pp. 24-76, 1966.
- [4] G. Brindly and W. Levin, "The sensation produced by electrical stimulation of the visual cortex," *J. Phys.*, vol. 195, pp. 479-493, 1963.
- [5] C. P. Ledergerber, "Postoperative electroanalgesia," *Obstet. Gynecol.*, vol. 51, pp. 334-338, Mar. 1978.
- [6] W. H. Ko, S. P. Liang, and C. D. F. Fung, "Design of radio-frequency powered coils for implant instruments," *Med. Biol. Eng., Comput.*, no. 15, pp. 634-640, 1977.
- [7] P. H. Peckham and J. T. Mortimer, "Restoration of hand function in the quadriplegic through electrical stimulation," in *Functional Electrical Stimulation, Application in Neural Prosthesis*, F. T. Hambrecht and J. B. Reswick, Eds. New York: Marcel Dekker, 1977, pp. 83-95.
- [8] P. H. Peckham, E. B. Marsolais, and J. T. Mortimer, "Restoration of key grip and release in the C-6 quadriplegic through functional electrical stimulation," *J. Hand Surg.*, vol. 5, pp. 462-469, 1980.
- [9] P. H. Peckham, C. W. Poon, W. H. Ko, E. B. Marsolais, and J. J. Rosen, "Multichannel implantable stimulator for control of paralyzed muscle," *IEEE Trans. Biomed. Eng.*, vol. 28, no. 7, pp. 112-116, July 1981.
- [10] B. Smith, P. H. Peckham, M. W. Keith, and D. D. Roscoe, "An externally powered, multichannel, implantable stimulator for versatile control of paralyzed muscle," *IEEE Trans. Biomed. Eng.*, vol. BME-34, no. 7, pp. 499-508, 1987.
- [11] P. R. Troyk and J. Poyezdala, "A four-channel implantable neuromuscular stimulator for functional electrical stimulation," in *Proc. 9th Annu. Conf. IEEE-EMBS*, 1987, pp. 620-621.
- [12] P. M. Meadows, D. R. McNeal, N. Y. Su, and W. W. Tu, "Development of an implantable electrical stimulation system for gait applications in stroke and spinal cord injured patients," in *Proc. 9th Annu. Conf. IEEE-EMBS*, 1987, pp. 618-619.
- [13] M. W. Keith, P. H. Peckham, G. B. Thrope, K. C. Stroh, B. Smith, J. R. Bucket, K. L. Kilgore, and J. W. Jatich, "Implantable functional neuromuscular stimulation in the tetraplegic hand," *J. Hand Surg.*, vol. 14A, pp. 524-530, 1989.
- [14] G. E. Loeb, C. J. Zamin, J. H. Schulman, and P. R. Troyk, "Injectable microstimulator for functional electrical stimulation," *Med. Biol. Eng., Comput.*, pp. NS13-NS19, Nov. 1991.
- [15] B. Ziaie, M. Nardin, J. Von Arx, K. Najafi, "A single-channel implantable microstimulator for functional neuromuscular stimulation," in *Proc. 7th Int. Conf. Solid State Sensors and Actuators*, Yokohama, June 1993, pp. 450-453.
- [16] N. O. Sokal and A. D. Sokal, "Class E: A new class of high-efficiency tuned single-ended switching power amplifiers," *IEEE J. Solid-State Circuits*, vol. SC-10, no. 3, pp. 168-176, June 1975.
- [17] T. Akin, B. Ziaie, and K. Najafi, "RF telemetry powering and control of hermetically sealed integrated sensors and actuators," in *Tech. Dig., IEEE Solid-State Sensors and Actuators Workshop*, Hilton Head, SC, June 1990, pp. 145-148, .
- [18] J. T. Mortimer, "Electrical excitation of nerve," in *Neural Prostheses, Fundamental Studies*, W. F. Agnew and D. B. McCreery, Eds. Englewood Cliffs, NJ: Prentice-Hall, 1990.
- [19] K. R. Foster, "Electromagnetic field effects and mechanisms," *IEEE Eng. Med. Biol. Mag.*, vol. 15, no. 4, pp. 50-56, July/Aug. 1996.
- [20] H. A. Haus and J. R. Melcher, *Electromagnetic Fields and Energy*. Englewood Cliffs, NJ: Prentice-Hall, 1989.
- [21] K. R. Foster and H. P. Schwan, "Dielectric properties of tissues," in *Handbook of Biological Effects of Electromagnetic Fields*, C. Polk and E. Postow Eds. Boca Raton, FL: CRC, 1996.
- [22] A. W. Guy, J. F. Lehmann, and J. R. Stonebridge, "Therapeutic applications of electromagnetic power," *Proc. IEEE*, vol. 62, no. 1, pp. 55-75, Jan. 1974.
- [23] P. R. Gray and R. G. Meyer, *Analysis and Design of Analog Integrated Circuits*. New York: Wiley, 1993.
- [24] J. Ji and K. D. Wise, "An implantable CMOS circuit interface for multiplexed microelectrode recording array," *IEEE J. Solid-State Circuits*, vol. 27, no. 3, pp. 433-443, Mar. 1992.
- [25] B. Ziaie, Y. Gianchandani, and K. Najafi, "A high-current IrOx thin-film neuromuscular microstimulator," in *Proc. 6th Int. Conf. Solid-State Sensors and Actuators*, June 1991, San Francisco, pp. 124-127.
- [26] J. D. Wiley and J. G. Webster, "Analysis and control of the current distribution under circular dispersive electrodes," *IEEE Trans. Biomed. Eng.* vol. BME-29, no. 5, pp. 381-385, May 1982.
- [27] L. S. Robblee, J. L. Lefko, and S. B. Brummer, "Activated iridium: An electrode suitable for reversible charge injection in saline solution," *J. Electrochem. Soc.*, vol. 130, pp. 731-733, 1983.
- [28] J. D. Wiley and J. G. Webster, "Distributed equivalent-circuit models for circular dispersive electrodes," *IEEE Trans. Biomed. Eng.*, vol. BME-29, no. 5, pp. 385-389, May 1982.
- [29] J. T. Rubenstein, F. A. Spelman, M. Soma, and M. F. Susserman, "Current density profile of surface-mounted recessed electrodes for neural prosthesis," *IEEE Trans. Biomed. Eng.*, vol. BME-34, no. 11, pp. 864-875, Nov. 1987.
- [30] B. Ziaie, J. A. Von Arx, and K. Najafi, "A micro-fabricated planar high-current IrOx stimulating microelectrode," in *Proc. 18th Ann. Conf., IEEE-EMBS*, Amsterdam, 1996, pp. 653.
- [31] G. Wallis and D. I. Pomerantz, "Field-assisted metal-glass bonding," *J. Appl. Phys.*, vol. 40, pp. 3946-3949, 1969.
- [32] J. Von Arx, B. Ziaie, M. Dokmeci, and K. Najafi, "Hermeticity testing of glass-silicon packages with on-chip feedthroughs," in *Proc. 8th Int. Conf. Solid-State Sensors and Actuators*, Stockholm, June 1995, pp. 244-247.
- [33] B. Ziaie, J. A. Von Arx, M. R. Dokmeci, and K. Najafi, "A hermetic glass-silicon micropackage with high-density on-chip feedthroughs for sensors and actuators," *IEEE J. Microelectromech. Syst.*, vol. 5, no. 3, pp. 166-179, Sept. 1996.
- [34] A. C. Adams, "Dielectric and polysilicon film deposition," in *VLSI Technology*, S. M. Sze, Ed. New York: McGraw Hill, 1988.



Babak Ziaie (A'95) received the B.S.E.E. degree from Tehran University, Tehran, Iran, in 1986 and the M.S. and Ph.D. degrees from the University of Michigan, Ann Arbor, in 1992 and 1994, respectively. His Ph.D. dissertation concentrated on the design and development of a single-channel microstimulator for functional neuromuscular stimulation.

In 1994–95 he was a Postdoctoral Research Fellow at Cardiac Rhythm Management Laboratory at the University of Alabama, Birmingham, where he was involved in developing high-density recording electrode arrays for mapping cardiac arrhythmia. Since 1995 he has been a Research Scientist at the Center for Integrated Sensors and Circuits, Department of Electrical Engineering and Computer Science, University of Michigan, where he has been involved in research and development of integrated sensors and actuators, microstructures, microtelemetry systems for biomedical applications, and packaging and encapsulation of implantable sensors. His major areas of interest include solid-state integrated sensors, micromachining technologies, VLSI and custom integrated circuits, instrumentation, and biotelemetry.

Dr. Ziaie is a member of Tau Beta Pi.



Mark D. Nardin was born in Grand Rapids, MI, on January 11, 1967. He received the B.S. degree in electrical engineering from Michigan Technological University, Houghton, in 1989, the M.S. degree from Princeton University, Princeton, NJ, in 1990, and the Ph.D. degree in electrical engineering from the University of Michigan, Ann Arbor, in 1996.

Since February 1996, he has been working in the field of circuit design for microprocessors at Intel Corp. in Hillsboro, OR. His interests include analog and digital circuit design.

Dr. Nardin is a member of Eta Kappa Nu.



Anthony R. Coghlan (S'91–M'97) was born in Santiago, Chile, in 1970. He received the B.S.E.E. degree (summa cum laude) from Vanderbilt University, Nashville, TN, in 1993 and the M.S.E.E. from the University of Michigan, Ann Arbor, in 1995. Currently he is a doctoral student and research assistant in the Center for Integrated Sensors and Circuits/Solid State Electronics Laboratory of the University of Michigan, researching wireless, implantable systems for functional neuromuscular stimulation.

His interests include mixed-mode circuit design, communication and signal processing theory and systems, and solid state theory and its applications. He is also an amateur musician and artist with strong interest in sound and image processing.

Mr. Coghlan's is a member of Tau Beta Pi and Eta Kappa Nu.



Khalil Najafi (S'84–M'85) was born in 1958 in Iran. He received the B.S.E.E. degree in 1980 and the M.S.E.E. degree in 1981, both from the University of Michigan, Ann Arbor. He obtained the Ph.D. degree in electrical engineering from the University of Michigan in 1986.

From 1986 to 1988 he was employed as a Research Fellow, from 1988 to 1990 as an Assistant Research Scientist, from 1990 to 1993 as an Assistant Professor, and since September 1993, as an Associate Professor in the Center for Integrated Sensors and Circuits, Department of Electrical Engineering and Computer Science, University of Michigan. His research interests include the development and design of: solid-state integrated sensors and microactuators; analog and digital integrated circuits; implantable microtelemetry systems and transducers for biomedical applications; technologies and structures for micro electromechanical systems and microstructures; and packaging techniques for microtransducers.

Dr. Najafi was awarded a National Science Foundation Young Investigator Award from 1992–1997, was the recipient of the Beatrice Winner Award for Editorial Excellence at the 1986 International Solid-State Circuits Conference, and of the Paul Rappaport Award for co-authoring the Best Paper published in the IEEE TRANSACTIONS ON ELECTRON DEVICES. In 1994 he received the University of Michigan's "Henry Russel Award" for outstanding achievement and scholarship and was selected by students in EECS department as the "Professor of the Year" in 1993. He has been active in the field of solid-state sensors and actuators for more than ten years, and has been involved in the program committees of several conferences and workshops dealing with solid-state sensors and actuators, including the International Electron Devices Meeting, the Hilton-Head Solid-State Sensors and Actuators Workshop, and the IEEE/ASME Microelectromechanical Systems (MEMS) Workshop. Dr. Najafi is the Editor for Solid-State Sensors for IEEE TRANSACTIONS ON ELECTRON DEVICES, and an Associate Editor for the *Journal of Micromechanics and Microengineering* (Institute of Physics).